GRAVITY-DEPENDENT TRANSPORT IN INDUSTRIAL PROCESSES

Simon Ostrach and Yasuhiro Kamotani
Department of Mechanical and Aerospace Engineering
Case Western Reserve University
Cleveland, Ohio 44106

ABSTRACT

Gravity dependent transport phenomena in various industrial processes are investigated in order to indicate new directions for micro-gravity research that enhance the commercial success of the space program. The present article describes the commercialization possibilities of such topics associated with physicochemical transport phenomena. The topics are: coating flow, rotating electrochemical system, and convection in low Prandtl number fluids. The present study is directed to understand these phenomena, and to develop a knowledge base for their applications with emphasis to a micro-gravity environment.

INTRODUCTION

Ostrach (ref. 1) indicated new directions for micro-gravity research that could enhance the commercial success of the space program. In particular, it is pointed out that the research is dispersed over a number of disciplines but the underlying, and unifying basis for new and unusual aspects are gravitationally modified biophysicochemical transport phenomena. The important implications include the effects of fluid flow, heat and mass transfer on biology and chemical reactions. Inversely, the transport phenomena associated with such processes are different in a modified gravitational environment. Such phenomena are vital elements of the chemical, pharmaceutical, energy production, material processing, and biotech industries. The present results demonstrate a great potential for space applications.

Furthermore, ground-based research and the corresponding industrial applications in space have been identified. The present research effort has resulted in various topics. First, transport phenomena in zeolite growth were thoroughly investigated, and subsequently a method for increasing the crystal size by adding nutrient after crystallization was developed. Second, the effect of regular and random modes *g-jitter*, on liquid motion in an open container under microgravity environment was examined numerically and analytically. Third, a theoretical analysis of bubble formation in continuous liquid phase under both terrestrial and microgravity environments investigated though more experimental research is still under way. Fourth, an experimental study on double diffusive convection was completed. Fifth, a scaling and theoretical analysis were performed to understand transport phenomena in supercritical fluid extraction. To date, all these topics have been thoroughly investigated and a detail description can be found elsewhere (ref. 1 and 12). The current research topics are described individually in the following sections: rotating electrochemical systems, coating flows, and convection in low Prandtl number fluids.

ROTATING ELECTROCHEMICAL SYSTEMS

The present study shows that there is a need to increase mass transport by a rotating system to achieve a high density power system in micro-gravity. Ostrach et al., (ref. 2) completed scaling and experimental studies on natural convection in a shallow rotating annulus subjected to axial stable temperature gradient. The present work, in essence, is an extension of that study.

The present research was motivated by the discovery of a rotating nickel-zinc (Ni-Zi) battery system. The main advantages of this system include the following: a high specific energy (~80 KWh/Kg), an excellent power performance (~100^{+} KW/Kg), a good performance in cold ambient temperatures, inexpensive, and low toxicity materials. These excellent performance characteristics make a rotating battery a leading candidate for energy generation and storage in micro-gravity. The development and commercialization of stationary Ni-Zn battery have been hindered for decades mainly due to the limited life cycles. Failure of this battery is typically associated with two phenomena: First, zinc dendrite formation and propagation that leads to the cell shorting. Second, zinc material redistribution (or shape change), which leads to gradual capacity loss. Conversely, by rotating the battery, the following performance enhancements are noticed: First, at rotations corresponding to 50 times the earth's gravitation the dentrite growth is nearly eliminated. This

leads to the stabilization of the electrode morphology and the battery life is prolonged to well over 1000 cycles, which is an industrially accepted standard. Second, the discharging electrical current density is increased by a factor of five.

Weng et al., (ref. 7) have experimentally and numerically studied the solutal convection inside shallow rotating electrochemical cell subject to concentration difference between two electrodes. A dilute binary electrolyte, cupric-sulfate system is the working fluid in both experimental and numerical simulations. The limiting current method is used to measure the mass transfer rate in cells. Numerical analysis is limited to cases when the flow is axisymmetric and laminar. The Boussinesq approximation is adopted for the centrifugal thermal buoyancy term in the numerical model. The basic equations with their appropriate boundary conditions are discretized and solved by SIMPLEC scheme to obtain velocity fields, concentration profiles, and local and average mass transfer rates at the electrodes.

The following non dimensional parameter characterize the rotating battery upper range: an Ekman number, $Ek=\nu/(\Omega H)^2$ ($\sim 1.07\times10^{-3}$), a solutal Rossby number, $Ro_m=\beta_m\Delta C$ ($\sim 2.24\times10^{-3}$), $Ra_\Omega=\Omega^2\beta\Delta C R^4/\nu\alpha$ ($\sim 2.63\times10^{11}$), a centrifugal Rayleigh number, a Schmidt number, $Sc=\nu/D$ (*~2380*), an aspect ratio, $Ar=H/R$ ($\sim 1/15$), and a Froude number, $Fr=R\Omega^2/g$ ($Fr>1$) (where Ω is the speed in rad/s; β_m is the concentration expansion coefficient; D is diffusivity; H the height of the cell). In the present parametric ranges Ekman and centrifugal buoyancy-driven flows have been identified. Although centrifugal buoyancy and Coriolis force increased simultaneously with Ro_m, the increase rate of the former was greater than that of the latter. *Figure 1* shows the dependency of the overall mass transfer rate on the centrifugal Rayleigh number. This figure shows that the present results agree well with the scaling law derived by Ostrach et al., (ref. 2) and the experimental results obtained by Hudson et al., (ref. 8). The combined uncertainty using the root sum square method in the determination of the *Ra* is ±10 %, *Fr* is ±2%, and the *Sh* is ±10%.

The present work has classified into two categories the flow structure and the concentration distribution. First, at relatively low rotation speed, the core flow is mainly unicellular. *Figure 2a* shows unicellular flow sandwiched between two Ekman layers; one near the top wall, and the other at the bottom, also demonstrated by the steep concentration of iso-solute lines in *Figure 2b*. Second, when the rotation speed exceeds a critical value, or whenever the *Ek* is less than a certain value, a series of secondary flow cells appears in the core region as demonstrated in *Figure 2b*. The secondary flow is induced by Coriolis force, and its direction is opposite to the primary flow. Since the Coriolis force opposes the centrifugal buoyancy force, the centrifugal buoyancy is greatly weakened in the core region, causing the flow direction to change. The interaction between the core flow and the strong flow motion in the Ekman layer leads to the formation of the multiple cell flow structure. However, the multiple flow cells mainly occur in the core region, hence their influence on the mass transfer rate on electrodes is weak. This conclusion is portrayed in *Figure 3* which shows the numerical local Sherwood number Sh_H against the *r/R*. Farther increase in rotation speed causes the secondary cells to interact with the Ekman layer leading to unsteady, or turbulent flow. It is evident from *Figure 3* that the centrifugal buoyancy force enhances the mass transfer rate to the electrodes. This fact is used for the following conclusions: Since the local mass transfer to the electrode can be controlled, then shape-change effects are stabilized. This leads to increase the charging and discharging life cycle and gives a high specific power. The present results are beneficial to an optimal design of rotating batteries although more work is being pursed to obtain a better understanding of the stability and performance characteristics at higher gravitational levels.

COATING FLOW

Industrial coating processes involve covering surfaces with one or more uniform liquid layers which are subsequently cured or dried to form films. A major problem faced in these processes is the stability of the coating film before the curing process occurs. Recently, a renewed interest in coating flow has emerged because of new economically significant technologies, for instance the use coating flow in semiconductor industry. Correspondingly, there is a need to improve productivity, economy, and uniformity in the traditional coating process (for example photography films, and paper, X-ray films, paper, welding, galvanized steel, and laminated composites).

In these processes, the final film thickness can be very thin and must be highly accurate. Productivity reasons strive for high speed applications, and several discrete film layers are at times applied simultaneously. As a result of such demands, attempts to use a specific coating process for a given application frequently fail. The liquid layer may not be continuous and, if it is, waves or streaks may occur. Also, numerical and experimental studies on coating flow, show that the final film thickness in micro-gravity can be made much larger with greater precision. The present experimental and

numerical data indicates that gravity significantly influences the stability of a coating film. The coating film exhibits interfacial instability beyond a certain Reynolds number. Ultimately, the coating film becomes wavy (ref. 4 and 5).

The present work explores coating flow at high parametric ranges (high capillary number, $Ca=\mu U/\sigma$, and high Reynolds number $Re=Uh_o/\nu$, property number $Po=\mu(g/\rho\sigma^3)^{1/4}=\{(Ca/Re)*(h_o/h_\sigma)\}^{1/2}$), strongly motivated by practical considerations. (Where ν is the kinematic viscosity; σ is the surface tension at the liquid-air interface; U is the substrate withdrawal rate; h_o is the final film thickness; and h_σ is the capillary rise height.) The following non dimensional parameters characterize the coating flow range for the aforementioned industrial applications: $Ca \sim 1.0x10^{-3}$ *to* 4.0; $Re \sim 3.0x10^{-3}$ *to* 2.0; $Po \sim 8.0x10^{-2}$ *to* 257.0.

The results presented in *Figure 4* are based on experimental work described in detail by Kizito et al. (ref. 5). The combined uncertainty using the root sum square method in the determination of the Ca is ±1.2%, and the Re is ±1.23%. *Figure 4* depicts the following trends: First, beyond a certain Ca, the non dimensional film thickness becomes constant independent of Ca. Second, there is a final film thickness dependency on the Re expressed by a fluid Po. For instance, at Ca=0.1, and P=5.6 with a higher Re has the non-dimensional final film thickness $T_o(=(\rho g h_o^2/\mu U_o)^{1/2})$=0.69. The same Ca=0.1, gives T_o=0.54 for Po=53.0. *Figure 4* shows that beyond a certain Po=26, the non-dimensional final film thickness ceases to depend on the Re. Also, *Figure 4* compares the present work with the experiment of Lee et al., (ref. 9), and the theoretical relationship obtained by Levich. The figure shows that Levich's theoretical relationship ($T_o=0.93Ca^{1/6}$) used extensively in the past, does not hold for the most part of the present work. The new aspects *Figure 4* presents are: beyond a certain Ca, T_o becomes constant independent of Ca, and a dependency of T_o on the Re. In general, the figure reveals that when the Re_r ($Re_r=\rho^2 g h_o^3/3\mu^2$) exceeds unity, a dip coating film becomes unstable. The Re_r measures the magnitude of gravity induced shear in the final film region.

In most work to date the interface shape at liquid line has been assumed to be described by a static meniscus equation. However, a new aspect of importance to the stability and the understanding of coating flow is shown in *Figures 5, and 6*. These figures show the meniscus deformation at the liquid pool lines, identified as the apparent cusp formation. *Figure 5* shows an interfacial profile at: Po=5.6, Ca = 0.4, and Re = 19.5, and the profile is obtained experimental by optically sectioning the coating flow field at the line. *Figure 6* shows the region occupied by the fluid, its meniscus, streamlines and velocity vectors when the parameters are: Ca=4.1, and Re=6.5, consequently simulating a fluid with Po=53.0. The numerical solution is obtained using a Fluent Nekton code. The cause of the apparent cusp on the interface is attributed to the inertia effect of the return flow. The results obtained in this study can be used to design an optimal coating device although more work is needed to confirm the cause of the wavy motion. The wavy motion in the final film region is mainly attributed to gravity induced shear, although gravity induced return flow causing the apparent cusp or a capillary gradient may have a role. In order to test these assertions, a microgravity environment will allow one to sort out the gravity induced shear instability from that caused by a capillary gradient.

CONVECTION IN LOW PRANDTL NUMBER FLUIDS

Industrial crystal growth processes involve solidification of melt at significantly high temperature gradients. At these temperature gradients, natural convection can have a profound influence on the structure, and quality of the final solid phase. Specifically, oscillatory or time dependent convection in the liquid phase is undesirable because it results in periodic inhomogeneities in the final crystals. For example, compositional variations of a few percentages down to a sub-micron length scale affect the performance, the properties of the doped semi-conductors, and the structural integrity of alloy materials. Since semi-conductor crystals are a very important component of the electronic industry, it is worthwhile to seek a control strategy that will lead to the reduction of these periodic inhomogeneities. The control strategy requires a good understanding of the detailed physics of the transport phenomena in liquid metals which are used to simulate semi-conductor materials in their liquid phase. Natural convective flow of a low-Pr fluid develops fluctuations in the temperature outside the viscous boundary layer, which in many cases result in unsteady or oscillatory flows. These phenomena are inherently non-linear making analysis very difficult. Therefore, a combination of experimental and numerical approaches is used in the present study.

The present study is an extension of work by Kamotani et al., (ref. 6) who investigated natural convection of a liquid metal in cylinders whose wall ends are differentially heated. In particular, the present work is designed to investigate

convection in a simulated floating zone melting technique, which is one of the major configurations used in industrial crystal growth processes. The present experiments cover a wider range of Ar (aspect ratio) than those used in the crystal growth technique in order to study oscillatory convection under more general conditions. Thermocouples are placed in different azimuthal positions along the wall to detect the onset of oscillations, and to determine the oscillation flow structures and frequencies. The non-dimensional parameter range for the present study is: $Ra >> 1$, $Ar > 1$, $Pr < 1$, $Hr < 1$. Ra^* ($Ra^* = g\beta\Delta T(L/2)^3/\nu\alpha$) is a Rayleigh number based on a half of the height, and Hr is a relative heating zone size. *Figure 7* schematically shows the present experimental configuration; a detailed description is by Selver et al., (ref. 10). A data acquisition system by Keithley Instruments is used to convert the thermocouple outputs to digital values. Real time computer graphics generated by Labtech are used to determine the onset of oscillations. The critical temperature difference value for the onset of oscillation is reproducible within ±10%.

The critical Rayleigh number values for the onset of oscillation are presented in *Figure 8*. The present data are compared with those measured by other investigators (ref. 6 and 11) whose configuration is heated-from-below. Good agreement is obtained although the basic flow changes below $Ar^*=3$ in the present configuration. The change in the basic flow can be attributed to two flow structures before oscillations appear. The flow structures have been identified as unicellular and axisymmetric flow. To rule out non-uniformity as an influence on the critical values, the test section was tilted about 5 degrees, and no change in Ra_{cr} values was observed within experimental error. Temperature oscillation pattern and the corresponding frequency are presented in *Figure 9*. The figure shows the power spectrum versus the frequency and the temperature versus time for $Ar^*=2$. The frequency values are obtained using a Fast Fourier Transform to the thermocouple outputs. The study of the amplitude and phase of temperature traces at different azimuthal position reveals the aforementioned the convective flow structure. The oscillation modes also correspond to these two basic flow structures before oscillation. First, whenever Ar^* is large, the oscillations are due to the fact that the unicellular motion is rotating back and forth. Second, when Ar^* is below 3, the oscillation pattern is associated with a rotating non-axisymmetric toroidal pattern around the axis.

REFERENCES

1. Ostrach, S. , "Industrial Processes Influenced by Gravity," NASA CR-182140, C-21066-G. 1988
2. Ostrach, S., Gulic, I., Kamotani, Y., and Jiang, H. D., "Thermal Convection in A Shallow Rotating Annulus," 18th International Congress of Theoretical and Applied Mechanics, Haifa, Israel, August. 1992
3. Ostrach, S. Kizito, J. P., and Kamotani, Y., "Free Coating Flow at High Capillary and "Free Coating flow at High Capillary and Reynolds numbers," AMD-Vol. 184, ASME, 1995, pp 1-11.
4. Kizito, J. P., Ostrach, S., and Kamotani, Y., "Coating Flows In Micro-gravity," M.S. Thesis, Case Western Reserve University, Cleveland. 1991
5. Kizito, J. P., Ostrach, S., and Kamotani, Y., "Free Coating Flow at High Capillary and Reynolds Numbers," Ph.D. Thesis, Case Western Reserve University, Cleveland. 1995
6. Kamotani, Y., Weng, F. B., Ostrach, S., and Platt, J., "Oscillatory Natural Convection of a Liquid Metal in Circular Cylinders," Journal of Heat Transfer, Vol. 116, 1994, pp. 627-632.
7. Weng, F. B., Ostrach, S., and Kamotani, Y., Ph.D. Thesis, "Rotating Electrochemical Systems," Case Western Reserve University, Cleveland. 1996
8. Hudson, J. L., Tang, D. and Abell, S., ," Experiments on Centrifugally Driven Thermal Convection in a Rotating Cylinder," J. Fluid Mech., V.86, Part 1, 1978, pp. 147-159.
9. Lee, C. Y. and Tallmadge, J. A., "Dynamic Profile Data at Low Capillary Numbers," Ind. Eng. Ch. Fundamentals, Vol. 13, No. 4, pp 356-360., 1974.
10. Selver, R., Kamotani, Y., and Ostrach, S., "Convection In Low Prandtl Number Fluids," Ph.D. Thesis, Case Western Reserve University, Cleveland. 1996

11. Muller, G., Neumann, G., and Weber, W., "Natural Convection in Vertical Bridgman Configurations," Journal of Crystal Growth, Vol. 70, 1984, pp. 78-93.

12. Ostrach, S., and Kamotani, Y., "Gravity-dependent Transport in Industrial Processes," 2nd Microgravity Fluid Physics Conference, NASA Pub. 3276, 1994.

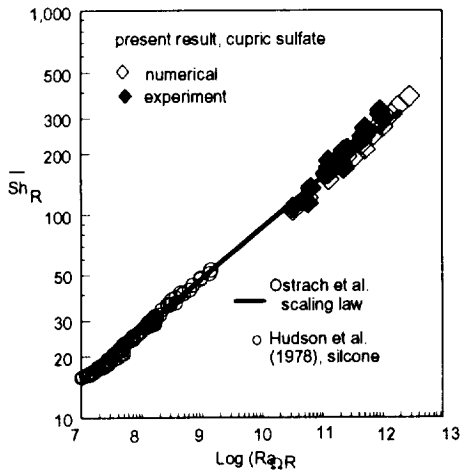

Figure 1 Cent. Rayleigh number vs. Sherwood number for present and published data

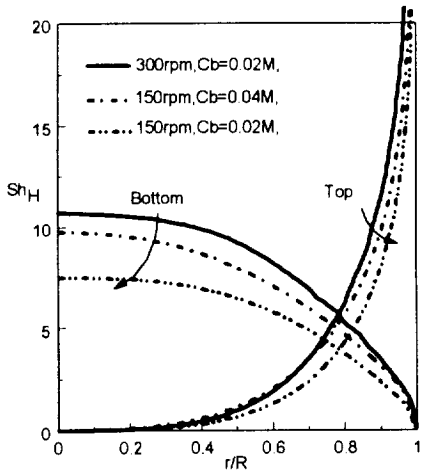

Fig. 3 Local Sherwood number distribution for Ar=0.0333 (numerical caculation)

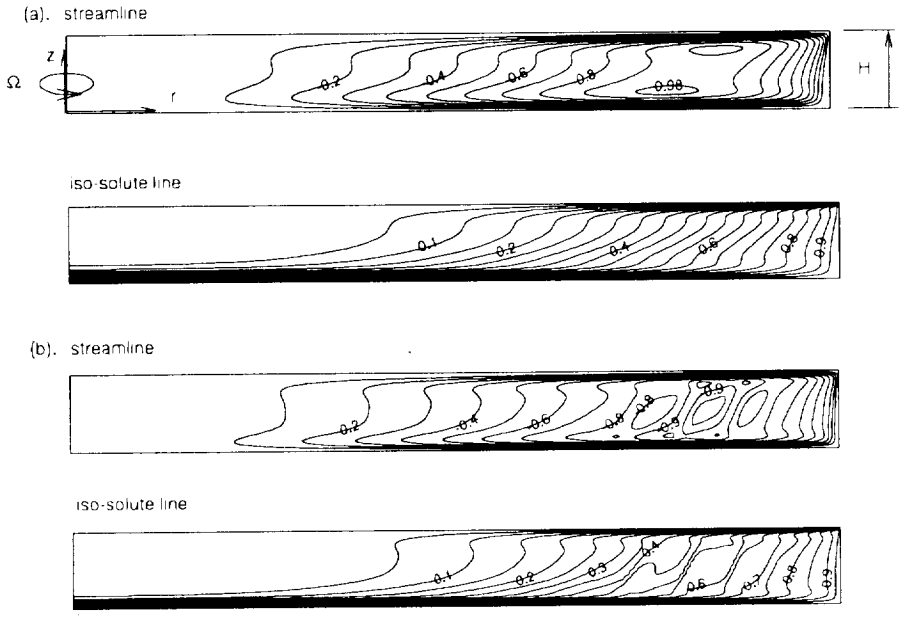

Figure 2 Contour plots of streamline, ios-solute line (vertical scale x3)
(a). Ω=150 rpm, ΔC=0.04M, $Ra_{\Omega R}$=6.58x10^{10}, Ek=0.0115, $ScRo_S$=10.63, Ar=0.033
(b). Ω=300 rpm, ΔC=0.04M, $Ra_{\Omega R}$=2.63x10^{11}, Ek=0.0057, $ScRo_S$=10.63, Ar=0.033

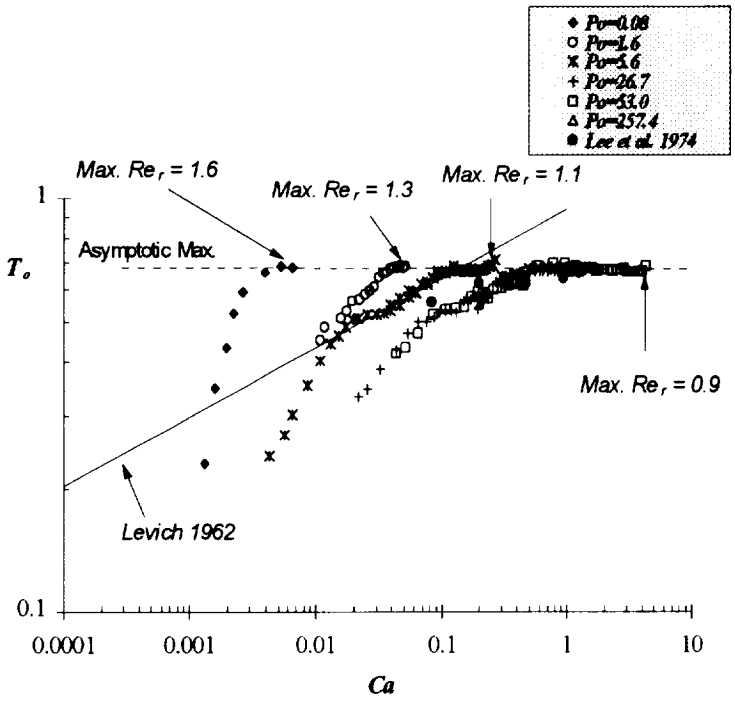

Figure 4: Non-dimensional final thickness as a function of Ca

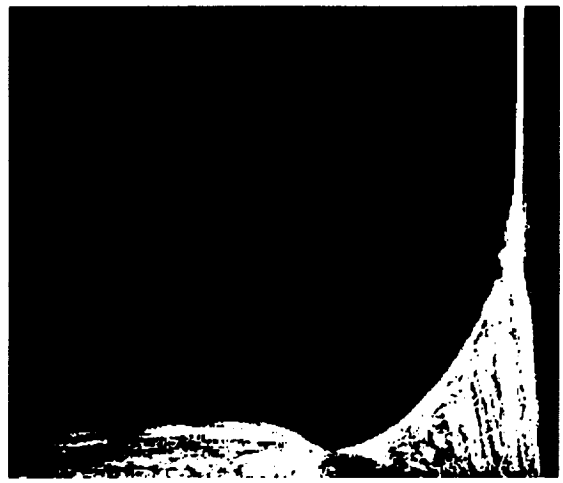

Figure 5: Interfacial profile at: Po=5.6, Ca = 0.4, and Re = 19.5

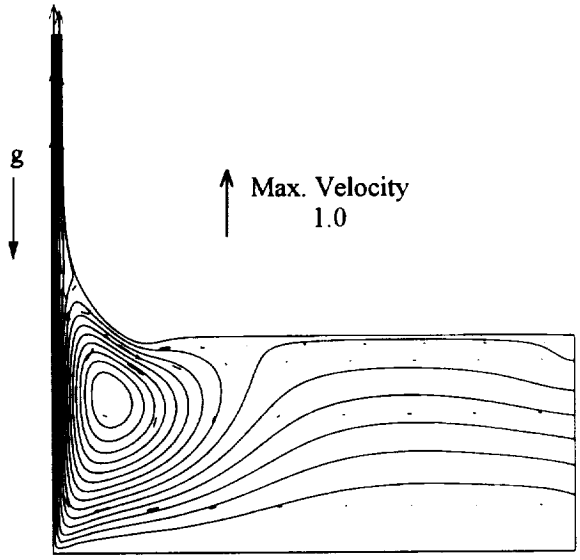

Figure 6: Numerical Interfacial profile at: Po=53.0, Ca = 4.1, and Re = 6.5

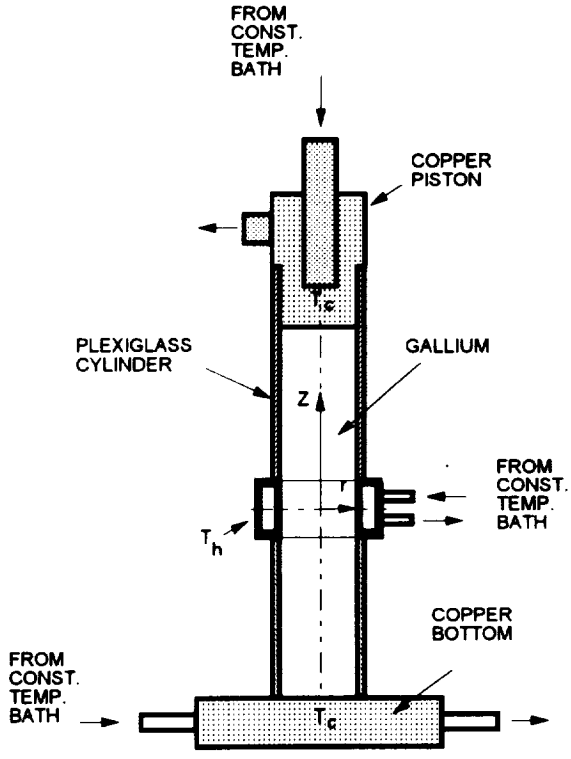

Figure 7: Experimental setup for convection in low Pr fluids

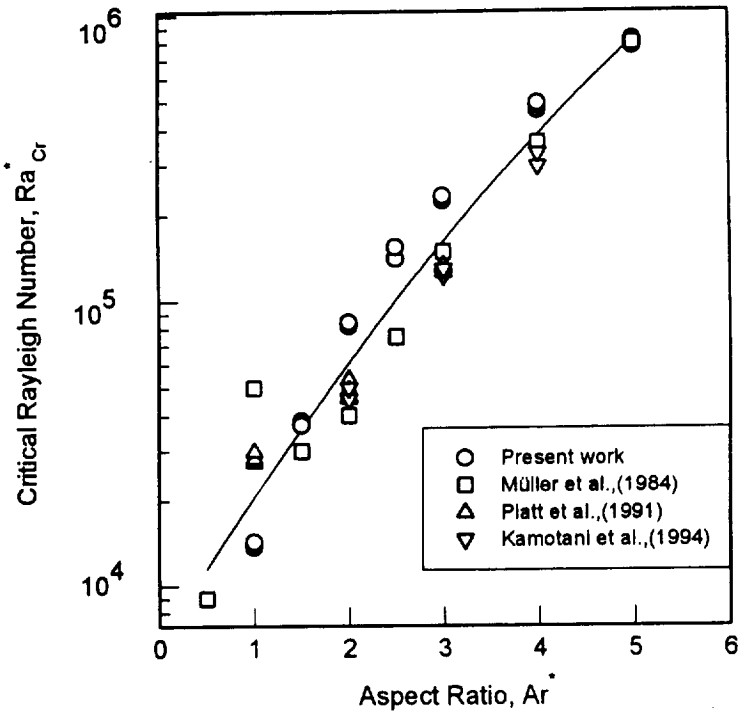

* Ra and Ar are based on the half of the test section height.

Figure 8 Comparison of critical Rayleigh numbers for vertical case with those of other investigators.

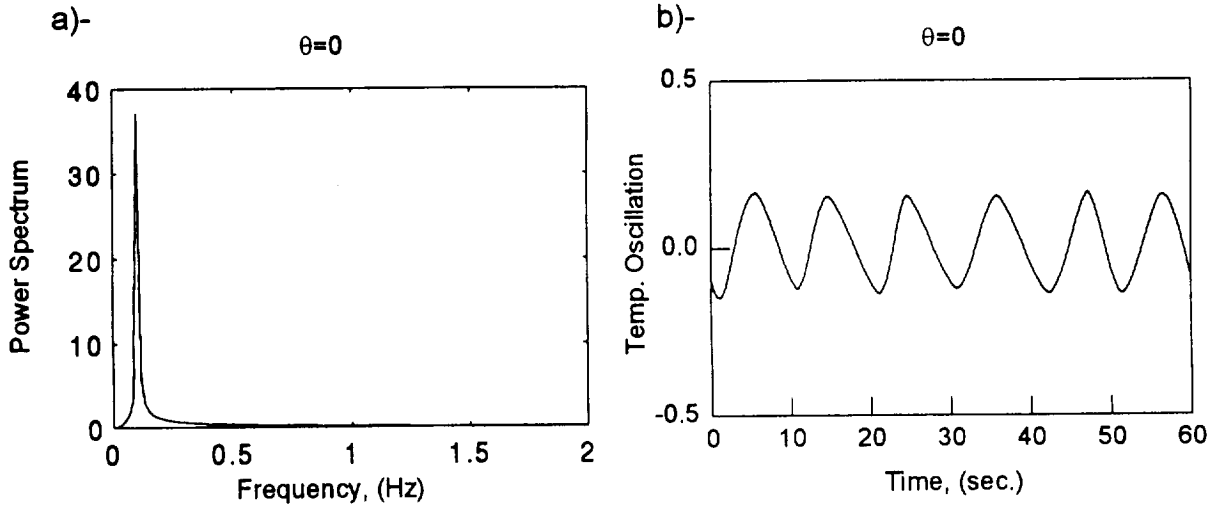

Figure 9 Temperature oscillations for Ar=2
a- Power Spectrums versus Frequency
b- Temperature traces versus Time